Journal of Molecular Graphics and Modelling 150 (2027) 109642

Contents lists available at ScienceDirect

Journal of Molecular Graphics and Modelling

journal homepage: www.elsevier.com/locate/jmgm

Structure-based discovery of novel BCL-X_L inhibitors through molecular docking and key interaction-guided virtual screening

Hyunjin Kim [a], Ahyoung Jang [b,c], Sungwoo Hong [b,c], Seong Eon Ryu [a,*], Hwangseo Park [d,**]

[a] Department of Bioengineering, College of Engineering, Hanyang University, 222 Wangsimri-rho, Seongdong-gu, Seoul, 04763, the Republic of Korea
[b] Department of Chemistry, Korea Advanced Institute of Science and Technology (KAIST), Daejeon, 34141, the Republic of Korea
[c] Center for Catalytic Hydrocarbon Functionalizations, Institute for Basic Science (IBS), Daejeon, 34141, the Republic of Korea
[d] Department of Bioscience and Biotechnology, Sejong University, 209 Neungdong-ro, Kwangjin-gu, Seoul, 05006, the Republic of Korea

ARTICLE INFO

Keywords:
Virtual screening
BCL-X_L inhibitor· apoptosis
Docking
Drug design

ABSTRACT

BCL-X_L, an anti-apoptotic member of the BCL-2 protein family, is an attractive therapeutic target for overcoming apoptosis resistance in cancer. However, the large, shallow, and predominantly hydrophobic nature of its BH3-binding groove has complicated the discovery of potent, drug-like small-molecule inhibitors. Here, we employed structure-based virtual screening with key interaction constraints to identify novel BCL-X_L inhibitor scaffolds with relatively low molecular weights (MWs). Approximately 312,000 drug-like compounds were docked into the BH3-binding groove, and the top-ranked molecules were filtered for simultaneous hydrogen-bond interactions with Ser106 and Arg139, yielding 26 candidates for experimental evaluation. Biochemical competitive binding assays identified two previously unreported inhibitors, **1** and **2**, with IC_{50} values of 0.34 and 2.51 μM, respectively. Both compounds possess relatively low MWs and moderate lipophilicity, providing favorable starting points for further medicinal chemistry optimization. Docking analyses indicated that both inhibitors occupy the canonical BH3-binding groove and are stabilized by the targeted hydrogen bonds with Ser106 and Arg139, together with extensive hydrophobic contacts. Notably, **1** forms an additional hydrogen bond with Arg139 through its benzo[c]isoxazole moiety, which may contribute to its higher potency. These findings establish **1** and **2** as novel BCL-X_L inhibitor scaffolds and support the use of key interaction constraints to improve docking-based virtual screening against challenging protein–protein interaction targets. Future studies will focus on structure-guided optimization of these scaffolds to strengthen their interactions within the BH3-binding groove, improve inhibitory potency toward the nanomolar range, and evaluate their cellular activity and drug-like properties.

1. Introduction

Dysregulation of apoptosis is a hallmark of cancer, contributing to uncontrolled cell proliferation and resistance to chemotherapy, radiotherapy, immunotherapy, and targeted therapies. The anti-apoptotic protein BCL-X_L, a key member of the BCL-2 family, promotes tumor cell survival by sequestering pro-apoptotic proteins and preventing mitochondrial outer membrane permeabilization [1]. Its frequent overexpression in a wide range of malignancies is closely associated with tumor progression, metastasis, and therapeutic resistance, making BCL-X_L an attractive target for anticancer drug discovery [2–4]. Consequently, the development of potent BCL-X_L inhibitors, either as selective agents or in combination with inhibitors of other anti-apoptotic BCL-2 family proteins, has emerged as a promising strategy for overcoming apoptosis resistance and improving cancer therapy [5,6].

Structurally, BCL-X_L belongs to the anti-apoptotic BCL-2 protein family and adopts a conserved α-helical fold comprising eight α-helices and four BCL-2 homology (BH) domains (BH1–BH4). The BH1, BH2, and BH3 domains collectively form a hydrophobic surface cleft, commonly referred to as the BH3-binding groove, which serves as the primary recognition site for the BH3 α-helices of pro-apoptotic proteins, including BAX, BAK, BIM, and BAD [7]. Through sequestration of these pro-apoptotic partners, BCL-X_L prevents mitochondrial outer membrane permeabilization and thereby suppresses apoptosis [8]. Consequently,

* Corresponding author.
** Corresponding author.
E-mail addresses: ryuse@hanyang.ac.kr (S.E. Ryu), hspark@sejong.ac.kr (H. Park).

https://doi.org/10.1016/j.jmgm.2026.109642
Received 21 August 2026; Received in revised form 20 October 2026; Accepted 1 November 2026
Available online 2 November 2026
1093-3263/© 2026 The Authors. Published by Elsevier Inc. This is an open access article under the CC BY license (http://creativecommons.org/licenses/by/4.0/).

disruption of protein–protein interactions within the BH3-binding groove has become the principal strategy for pharmacological inhibition of BCL-X_L. Despite its therapeutic importance, however, BCL-X_L has long been regarded as a challenging target for small-molecule drug discovery because the BH3-binding groove is a relatively large, elongated, and predominantly hydrophobic protein–protein interaction interface lacking well-defined deep binding pockets [9]. In addition, the conformational plasticity of several subpockets, particularly the P4 pocket, together with the extensive solvent exposure of the binding surface, further complicates the design of high-affinity ligands [10]. These structural characteristics have historically classified BCL-X_L as one of the representative "undruggable" protein targets and continue to present substantial challenges for the development of potent small-molecule inhibitors.

Over the past decade, considerable efforts have been devoted to the development of small-molecule BCL-X_L inhibitors despite the intrinsic challenges associated with targeting the large and shallow BH3-binding groove. These efforts have yielded a wide range of structurally diverse inhibitors, including ABT-737, AZD4320, WEHI-539, A-1331852, and numerous structurally related analogues (Fig. 1), many of which exhibit low-nanomolar and subnanomolar biochemical potency [11–22]. Several of these compounds have progressed to clinical evaluation, demonstrating the therapeutic potential of pharmacological BCL-X_L inhibition [23]. However, the clinical development of BCL-X_L inhibitors has been substantially constrained by mechanism-based, dose-limiting thrombocytopenia arising from the essential role of BCL-X_L in platelet survival [24,25]. This on-target toxicity can restrict systemic exposure and narrow the therapeutic window, prompting the exploration of alternative strategies. In addition to these safety concerns, many potent BCL-X_L inhibitors have high molecular weights (MWs), typically exceeding 500 atomic mass units (amu) and sometimes approaching 1000 amu, which can compromise their drug-like and pharmacokinetic properties [26]. This reflects the difficulty of achieving high-affinity binding to the expansive BH3-binding groove while maintaining favorable physicochemical properties. Even lower-MW inhibitors, such as BXI-72 (MW = 452.6 amu) [27], have not advanced to clinical evaluation despite excellent biochemical potency, demonstrating the challenge of balancing potency, pharmacokinetics, and safety. Therefore, the discovery of structurally distinct BCL-X_L inhibitor scaffolds that combine potent target inhibition with reduced MW and favorable drug-like properties remains an important objective in medicinal chemistry and may provide valuable starting points for the development of BCL-X_L-targeted therapeutics.

In this study, we sought to identify new classes of small-molecule inhibitors that disrupt the interaction between BCL-X_L and proapoptotic BH3 peptide ligands through structure-based virtual screening. The screening library was restricted to compounds with MWs below 500 amu to identify drug-like scaffolds suitable for subsequent chemical optimization. Although molecular docking is widely used for virtual screening, its predictive accuracy is limited by approximate scoring functions that cannot fully capture the energetic contributions to protein–ligand binding, often resulting in false-positive hits [28]. To improve hit selection, highly ranked compounds were therefore subjected to an additional structural filter requiring specific hydrogen-bonding interactions with experimentally validated hot-spot residues in the BCL-X_L BH3-binding groove. Thus, only compounds satisfying both the docking-score and key-interaction criteria were prioritized for experimental evaluation. This two-stage filtering strategy was expected to enhance the stringency of virtual screening and reduce false positives arising from the inherent limitations of empirical scoring functions.

2. Materials and methods

2.1. Preparation of all-atom receptor model for BCL-X_L

The receptor model for structure-based virtual screening was constructed from the X-ray crystal structure of BCL-X_L in complex with Cpd14 (Fig. 1), a highly potent small-molecule inhibitor structurally related to A-1331852 with a K_i value of 5 nM (PDB ID: 6VWC) [16]. The crystallographic structure was first processed to generate an all-atom

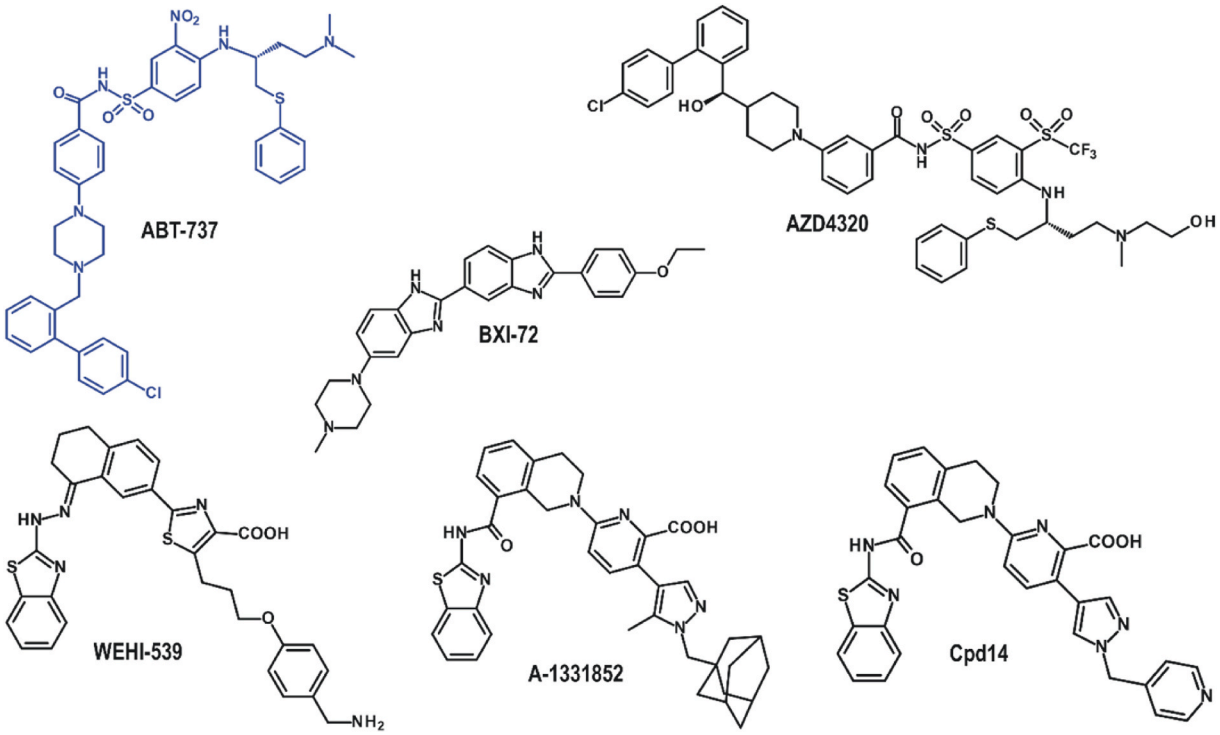


Fig. 1. Chemical structures of representative BCL-X_L inhibitors reported in the literature. ABT-737, shown in blue, was used as a reference compound for evaluating the BCL-X_L inhibitory activities of the candidate compounds identified through virtual screening.

representation of the protein suitable for molecular docking. Hydrogen atoms were added to all heavy atoms according to their local hybridization states, bonding environments, and expected protonation states under physiological conditions. Particular attention was given to ionizable amino acid side chains, as their protonation states can substantially influence the geometry and strength of protein–ligand interactions. Aspartate and glutamate residues were generally assigned in their negatively charged forms unless the local hydrogen-bonding environment favored protonation of a carboxylate oxygen. Similarly, the protonation states of lysine and histidine residues were determined based on their local electrostatic environments and involvement in hydrogen-bonding interactions. For histidine residues, the position of the proton on the imidazole ring was assigned to optimize the hydrogen-bonding network. The bound inhibitor and crystallographic water molecules were removed, whereas the experimentally determined protein conformation was retained to preserve the geometry of the ligand-binding pocket. The resulting protonated and chemically refined all-atom model of BCL-X_L was subsequently used as the receptor for molecular docking and virtual screening of a large chemical library to identify novel compounds capable of occupying the BH3-binding groove and thereby disrupting BCL-X_L interactions with proapoptotic BH3-domain-containing proteins.

$$\Delta G_{bind} = 0.1485\sum_{i=1}\sum_{j>i}\left(\frac{A_{ij}}{r_{ij}^{12}}-\frac{B_{ij}}{r_{ij}^{6}}\right)+0.0656\sum_{i=1}\sum_{j>i}E(t)\left(\frac{C_{ij}}{r_{ij}^{12}}-\frac{D_{ij}}{r_{ij}^{10}}\right)$$
$$+0.1146\sum_{i=1}\sum_{j>i}\frac{q_i q_j}{\varepsilon(r_{ij})r_{ij}}+0.3113N_{tor}+0.1711\sum_{i=1}\sum_{j>i}\left(S_i V_j+S_j V_i\right)e^{\left(-r_{ij}^2/2\sigma^2\right)} \quad (1)$$

2.2. Preparation of a chemical library for virtual screening of BCL-X_L inhibitors

A virtual chemical library was constructed from commercially available compounds in the InterBioScreen chemical database (https://www.ibscreen.com), which contains a diverse collection of synthetic and natural products suitable for structure-based virtual screening. Prior to molecular docking, all compounds were filtered according to Lipinski's Rule of Five to enrich the library with molecules possessing favorable drug-like properties and exclude those with a low likelihood of oral bioavailability [29,30]. Approximately 485,000 synthetic compounds and 69,000 natural products were initially collected and subjected to the Rule of Five criteria. Following this physicochemical filtering, approximately 312,000 structurally diverse compounds satisfying the predefined drug-likeness requirements were retained for subsequent molecular docking simulations.

All compounds in the virtual screening library were converted into three-dimensional (3D) structures using the CORINA program [31], which generates chemically reasonable atomic coordinates based on conformational rules and geometric parameters derived from experimentally determined small-molecule crystal structures in the Cambridge Structural Database. The resulting structures were used as the initial ligand conformations for docking. Partial atomic charges were then assigned to the ligands and the BCL-X_L receptor using the Gasteiger–Marsili method [32] to enable the calculation of intermolecular electrostatic interaction energies.

2.3. Docking simulations for prioritization of compounds in the virtual screening library

Molecular docking was performed with the AutoDock program [33], using AMBER force-field parameters to evaluate intermolecular van der Waals interactions and ligand internal conformational energies [34]. Each compound was docked into the BH3-binding groove of BCL-X_L and ranked according to its predicted binding affinity to prioritize potential BCL-X_L inhibitors. Binding affinity was evaluated using the empirical binding free-energy scoring function implemented in the original AutoDock program. The predicted binding free energy, ΔG_{bind}, was calculated from intermolecular protein–ligand interactions, the conformational penalty associated with ligand binding, and ligand desolvation, as expressed in Eq. (1).

The weighting coefficients for the van der Waals, hydrogen-bonding, electrostatic, torsional, and ligand desolvation terms were 0.1485, 0.0656, 0.1146, 0.3113, and 0.1711, respectively, according to the original AutoDock parameterization [33]. The hydrogen-bonding term includes an angular weighting function, $E(t)$, that accounts for hydrogen-bond directionality. In Eq. (1), r_{ij} denotes the distance between protein atom i and ligand atom j. Electrostatic interactions were evaluated using a sigmoidal distance-dependent dielectric function, $\varepsilon(r_{ij})$, to approximate dielectric screening in the protein environment [35]. The torsional term incorporates N_{tor}, the number of ligand rotatable bonds, to account for the conformational entropy penalty upon binding. In the desolvation term, S_i and V_i represent the atomic solvation parameter and fragmental atomic volume of atom i, respectively [36]. Collectively, the five terms in Eq. (1) provide an empirical estimate of binding free energy by accounting for the principal energetic contributions to protein–ligand complex formation.

For molecular docking, 3D interaction energy grids were calculated for all atom types recognized by the AutoDock force field. These grid maps were generated once for the BCL-X_L receptor and used for docking all compounds in the virtual library. The grid was centered at the center of mass of the co-crystallized inhibitor Cpd14 in the X-ray structure (PDB ID: 6VWC) [16] and consisted of 61 × 61 × 61 points with a spacing of 0.375 Å, defining a cubic search space extending 22.9 Å from the grid center. This region fully encompassed the BH3-binding groove and accommodated ligands of diverse sizes and conformations. All compounds were then docked into the BH3-binding groove and ranked according to their predicted binding free energies (ΔG_{bind}), from which the 100 highest-scoring compounds were selected for further analysis.

2.4. Application of configurational constraints to enforce interactions with hot-spot residues

To enrich for potential BCL-X_L inhibitors adopting binding modes similar to that of Cpd14, compounds were further required to form hydrogen bonds with the backbone carbonyl oxygen of Ser106 and the side-chain guanidinium group of Arg139, with donor–acceptor distances of <3.05 Å. These residues were selected as key interaction hotspots based on their characteristic hydrogen-bonding interactions with the co-crystallized inhibitor Cpd14. Although Asn136 also forms a hydrogen bond with Cpd14 through its side-chain amide group, this interaction appears to be weaker than those involving Ser106 and Arg139 [16] and was therefore not included as a hotspot interaction in the structure-based selection criteria.

2.5. Molecular dynamics (MD) simulations

MD simulations of BCL-X_L in complex with the newly identified inhibitors were performed using the AMBER 20 software package. Because force-field parameters for the inhibitors identified in this study were not available in the standard AMBER parameter database, the required parameters were derived according to the procedure described by Fox and Kollman [37], to maintain compatibility with the conventional AMBER force field. The initial structures of the BCL-X_L–inhibitor complexes were constructed from the binding conformations of the newly identified inhibitors obtained from the molecular docking calculations, with each inhibitor positioned within the BH3-binding groove of BCL-X_L.

For system preparation, three Na^+ counterions were introduced to neutralize the net charge of each BCL-X_L–inhibitor complex using the corresponding AMBER force-field parameters. Each resulting all-atom complex was subsequently immersed in a rectangular box of explicit TIP3P water molecules with dimensions of $60.9 \times 60.4 \times 66.8$ Å, yielding a solvated system containing 5545 water molecules. Prior to MD simulation, each solvated system was subjected to 2000 cycles of energy minimization to eliminate unfavorable steric contacts and relax the initial structure. The minimization consisted of 1000 steps using the steepest-descent algorithm, followed by an additional 1000 steps using the conjugate-gradient method.

Following energy minimization, the systems were equilibrated through a multistage protocol. Initially, the solvent molecules were equilibrated for 20 ps at 298.15 K while the solute atoms were restrained. The solute was then gradually equilibrated while maintaining the solvent configuration fixed, with the temperature increased stepwise through 10, 50, 100, 150, 200, 250, and 298.15 K. At each temperature, 10 ps of equilibration was performed to allow progressive relaxation of the solute and to minimize structural perturbations associated with rapid heating. After completion of the stepwise heating procedure, the entire solvated system was equilibrated for an additional 100 ps at 298.15 K without the preceding separation of solute and solvent equilibration.

Production MD simulations were subsequently performed for 20.4 ns at 298.15 K under periodic boundary conditions using the isothermal–isobaric (NPT) ensemble. The temperature and pressure were maintained at 298.15 K and 1 atm, respectively, throughout the production simulations. All covalent bonds involving hydrogen atoms were constrained using the SHAKE algorithm with a tolerance of 10^{-6} Å, permitting the use of an integration time step of 2.0 fs. A cutoff distance of 12 Å was applied to nonbonded interactions. The atomic coordinates were saved every 0.8 ps, corresponding to every 400 MD steps, to generate trajectories for subsequent structural and dynamic analyses. The same simulation protocol was applied to both BCL-X_L–inhibitor complexes to enable a consistent comparison of their dynamic behaviors.

2.6. Biochemical evaluation of BCL-X_L inhibitory activity

The biochemical inhibitory activities of the test compounds against BCL-X_L were determined by Reaction Biology Corp. (Malvern, PA, USA) using a homogeneous time-resolved fluorescence (HTRF) competitive binding assay. Compounds identified through virtual screening were purchased from InterBioScreen Ltd. (Bar, Montenegro), prepared as 10 mM stock solutions in DMSO, and initially screened at 10 μM. Compounds exhibiting >50% inhibition were selected for IC_{50} determination in duplicate using 3-fold serial dilutions starting at 100 μM. ABT-737 (Fig. 1) was used as the reference inhibitor and evaluated in parallel using 3-fold serial dilutions starting at 0.1 μM.

The assay measured competition between test compounds and a carboxyfluorescein (FAM)-labeled Bad peptide [38] for binding to glutathione S-transferase (GST)-tagged BCL-X_L, with the HTRF signal generated by energy transfer between the FAM-labeled peptide and an anti-GST terbium donor. The assay mixture contained 3 nM BCL-X_L and 40 nM FAM-Bad peptide in 20 mM potassium phosphate buffer (pH 7.5) containing 50 mM NaCl, 1 mM EDTA, 0.005% Triton X-100, and 1.0% DMSO. Test compounds were transferred to assay plates by acoustic liquid dispensing and incubated with BCL-X_L for 10 min at room temperature. FAM-Bad peptide was then added, followed by an additional 10 min incubation, after which anti-GST terbium donor reagent was added. HTRF signals were measured after a further 60 min incubation at room temperature. Raw fluorescence signals were background-corrected and converted to percentage binding relative to DMSO-treated controls. Concentration–response curves were fitted using GraphPad Prism, and IC_{50} values were determined for compounds exhibiting <65% residual binding at the highest concentration tested.

3. Results and discussion

3.1. Virtual screening and experimental identification of novel BCL-X_L inhibitors

Before structure-based virtual screening, the molecular docking protocol was validated using the crystal structure of the BCL-X_L–Cpd14 complex (PDB ID: 6VWC) [16], which served as the receptor model for subsequent docking simulations. As illustrated in Fig. 2, the protocol successfully reproduced the crystallographic binding mode of Cpd14 in the BH3-binding groove, with a root-mean-square deviation (RMSD) of 0.39 Å between the docked and experimental conformations. This RMSD value is well below the commonly accepted threshold of 2.0 Å for successful pose reproduction [39], supporting the reliability of the docking protocol for structure-based identification of novel BCL-X_L inhibitors.

Of the approximately 312,000 compounds docked into the BH3-binding groove of BCL-X_L, the top 100 ranked by predicted ΔG_{bind} were selected for further evaluation. As shown in Fig. 3, these compounds were subjected to an additional binding-mode filter to enrich for molecules capable of reproducing the key interactions of the reference ligand. Specifically, only compounds predicted to form hydrogen bonds with both the backbone carbonyl oxygen of Ser106 and the side-chain guanidinium group of Arg139 were retained, yielding 26 final virtual hits. All 26 compounds were commercially available from InterBioScreen Ltd. (Bar, Montenegro) and were purchased for biochemical evaluation. Their inhibitory activities against BCL-X_L were assessed by Reaction Biology Corp. (Malvern, PA, USA) using a competitive binding assay at an initial concentration of 10 μM. Of the 26 compounds tested,

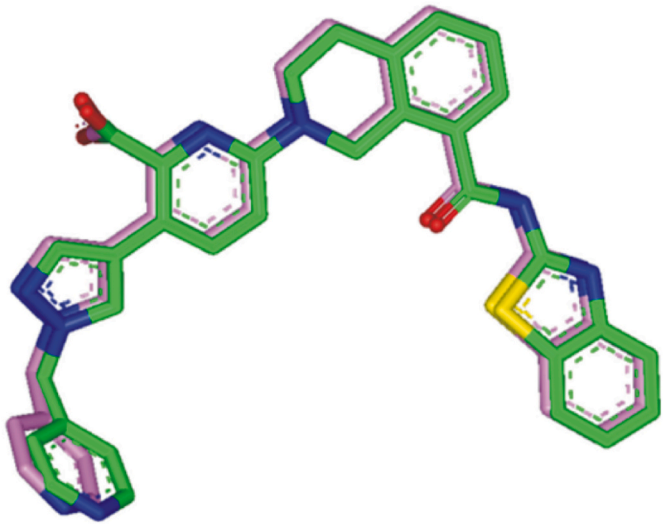


Fig. 2. Overlay of the crystallographic and docking-predicted binding conformations of Cpd14 within the BH3-binding groove of BCL-X_L. Carbon atoms are colored pink for the X-ray structure and green for the docked conformation.

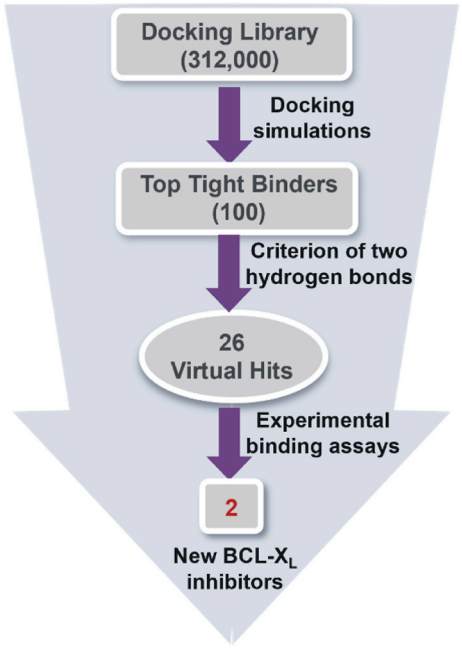


Fig. 3. Overall workflow of the structure-based virtual screening and subsequent biochemical validation strategy for the identification of novel BCL-X_L inhibitors.

two exhibited >50% inhibition and were subsequently selected for concentration–response studies.

The two hit compounds (**1** and **2**) were subsequently subjected to 10-point concentration–response assays to determine their IC_{50} values, with ABT-737 included as the reference inhibitor. The resulting concentration–response curves are presented in Fig. 4. Both **1** and **2** exhibited well-defined sigmoidal concentration–response profiles closely resembling that of ABT-737, demonstrating concentration-dependent inhibition of peptide binding to BCL-X_L. However, the concentration–response curves of both compounds were right-shifted relative to that of ABT-737, in agreement with the exceptionally high inhibitory potency of this reference inhibitor at the low-nanomolar level. With respect to the relative inhibitory potencies of the two compounds, **1** displayed a pronounced leftward shift compared with **2** (Fig. 4a), reaching the midpoint of the inhibition curve at a substantially lower concentration and exhibiting a steeper transition from minimal to maximal inhibition. Taken together, these concentration–response profiles indicate that **1** possesses substantially greater inhibitory potency than **2**.

3.2. *Structural and biochemical characterization of the newly identified BCL-X_L inhibitors*

The chemical structures of the two newly identified BCL-X_L inhibitors, **1** and **2**, are shown in Fig. 5. To the best of our knowledge, neither compound has previously been reported as a BCL-X_L inhibitor in the scientific or patent literature, supporting their structural novelty. Despite their distinct scaffolds, both compounds contain multiple hydrogen-bonding functionalities associated with aromatic and heteroaromatic moieties, including phenyl, triazole, and benzo[c]isoxazole groups. These features may promote hydrogen-bonding interactions with residues in the BH3-binding groove, while their aromatic ring systems can establish complementary hydrophobic and van der Waals contacts within the largely hydrophobic binding pocket. To assess the possibility of nonspecific assay interference, **1** and **2** were also screened for pan-assay interference compounds (PAINS) motifs [40,41]. Neither compound contained a recognized PAINS motif, reducing the likelihood that their observed activities resulted from common assay-interference mechanisms and further supporting their identification as genuine BCL-X_L screening hits.

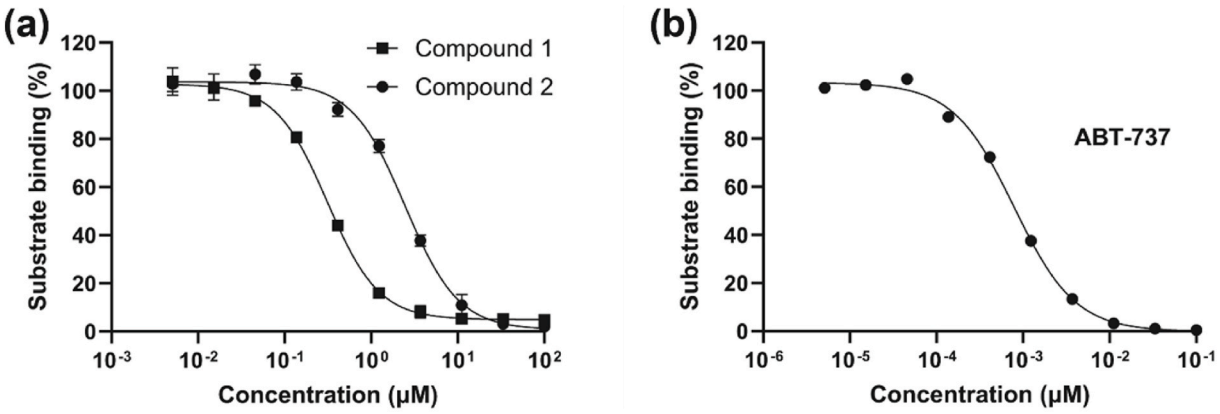


Fig. 4. Concentration–response curves used to determine the IC_{50} values for inhibition of peptide substrate binding to BCL-X_L by (a) **1** and **2**, and (b) ABT-737.

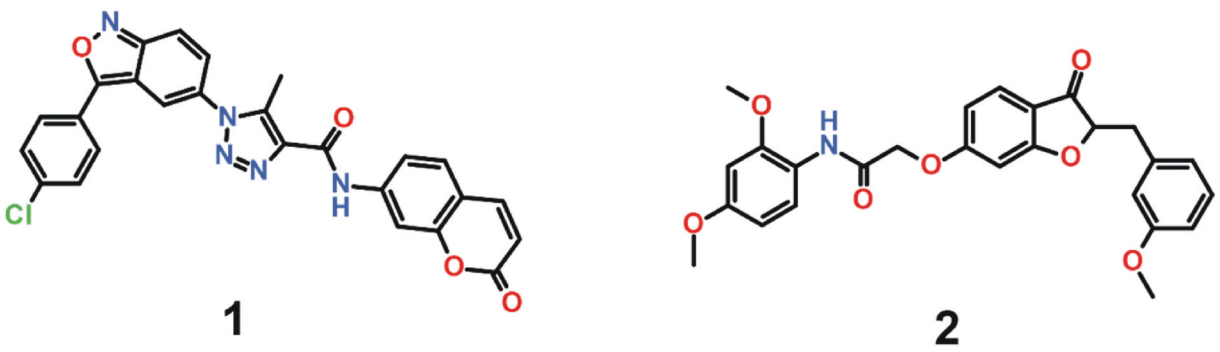


Fig. 5. Chemical structures of the two newly identified BCL-X_L inhibitors.

Table 1
Comparison of the IC_{50} values of **1** and **2** for inhibition of peptide binding to BCL-X_L, along with their MWs, calculated lipophilicities (cLogP), and predicted median lethal doses (cLD50), with those of the reference compound ABT-737.

compound	MW (amu)	cLogP	cLD50 (mg/kg)	IC_{50} (μM)
1	497.9	4.81	500	0.34 ± 0.01
2	463.5	4.12	500	2.51 ± 0.04
ABT-737	813.4	7.88	3014	0.0008

The biochemical inhibitory potencies of the two BCL-X_L hits are summarized in Table 1, together with MWs and calculated LogP (cLogP) values. **1** and **2** inhibited peptide binding to BCL-X_L with IC_{50} values of 0.34 and 2.51 μM, respectively. These activities are noteworthy given the challenging nature of BCL-X_L as a protein–protein interaction target, owing to its large and shallow BH3-binding groove, which complicates the discovery of high-affinity small-molecule inhibitors. The identification of two previously unreported inhibitors with submicromolar to-low-micromolar potencies therefore supports the effectiveness of the present computational strategy for identifying novel BCL-X_L inhibitor scaffolds.

Although the reference inhibitor ABT-737 exhibited substantially greater potency ($IC_{50} = 0.8$ nM), **1** and **2** represent structurally distinct scaffolds rather than close analogues of known BH3 mimetics, thereby expanding the chemical space available for BCL-X_L inhibitor development. Notably, both compounds have relatively low MWs compared with many reported BCL-X_L inhibitors, including ABT-737, which exceeds 800 amu. Compound **1** has an MW of 497.9 amu, while **2** is even smaller at 463.5 amu, satisfying Lipinski's MW criterion and providing greater scope for medicinal chemistry optimization. Their lower MWs may permit the introduction of potency-enhancing substituents while maintaining drug-like physicochemical properties. Moreover, their moderate lipophilicity (cLogP = 4.81 and 4.12 for **1** and **2**, respectively) provides additional scope for structural optimization without excessive increases in lipophilicity.

The submicromolar potency of **1** makes it an attractive lead for structure-activity relationship (SAR) studies aimed at developing more potent BCL-X_L inhibitors, whereas the lower MW of **2** provides greater scope for structural modification despite its weaker activity. Thus, both compounds represent promising starting points for the structure-based development of new BCL-X_L inhibitors. Their identification further supports the utility of the present virtual screening strategy for discovering novel inhibitor scaffolds against the challenging BCL-X_L protein–protein interaction interface.

To complement the biochemical evaluation of inhibitory potency, we also conducted an *in silico* toxicity assessment of **1** and **2**, alongside ABT-737 as a reference inhibitor, using the ProTox 3.0 platform [42] to estimate their potential acute toxicity and gain preliminary insights into their toxicological profiles. Specifically, we estimated the median lethal dose (LD50), defined as the dose of a substance expected to cause mortality in 50% of an exposed test population under specified experimental conditions. The computationally predicted LD50 (cLD50) values are expressed in milligrams per kilogram of body weight (mg/kg). As summarized in Table 1, both **1** and **2** exhibited a predicted cLD50 value of 500 mg/kg, with corresponding prediction confidence scores of 54.26% and 68.07%, respectively. According to the Globally Harmonized System of Classification and Labelling of Chemicals (GHS) [43], **1** and **2** were assigned to acute oral toxicity Category 4 ($300 < LD50 \leq 2000$ mg/kg), whereas ABT-737 was assigned to Category 5 ($2000 < LD50 \leq 5000$ mg/kg). These categories are associated with the hazard statements "Harmful if swallowed" and "May be harmful if swallowed," respectively. Thus, although both **1** and **2** were predicted to exhibit greater acute oral toxicity than the reference inhibitor ABT-737, neither was classified within the more severe acute toxicity categories (Categories 1–3). Nevertheless, their assignment to Category 4 indicates that potentially harmful effects following oral exposure cannot be excluded. It should be emphasized that these computational predictions represent preliminary estimates rather than experimentally validated toxicological findings and therefore cannot establish the safety of either compound. In particular, the predicted cLD50 values do not adequately account for organ-specific toxicity, cumulative toxic effects, chronic toxicity, or other adverse consequences associated with prolonged exposure. Furthermore, the identical cLD50 values predicted for **1** and **2** should not be interpreted as evidence of equivalent toxicological profiles, particularly considering the differences in their associated prediction confidence scores. Despite these limitations, the present findings provide an initial assessment of the potential acute toxicity liabilities of the newly identified inhibitors and suggest that both compounds may serve as starting points for further development, provided that their predicted toxicological risks are systematically evaluated and addressed.

3.3. *Predicted binding modes and molecular interactions of BCL-X_L inhibitors **1** and **2***

Based on their chemical structures (Fig. 5), the inhibitory activities of **1** and **2** may arise from a combination of directional hydrogen-bonding and hydrophobic interactions that stabilize their binding within the BH3-binding groove of BCL-X_L, thereby interfering with the binding of proapoptotic BH3 peptides. To gain structural insight into their inhibitory mechanism, the predicted binding modes of **1** and **2** were compared with the crystallographic pose of Cpd14. As shown in Fig. 6, both compounds were predicted to occupy the canonical BH3-binding groove in orientations similar to that of Cpd14, showing substantial structural overlap while preserving the key hydrogen bonds with Ser106 and Arg139. However, the terminal chromen-2-one moiety of **1** and dimethoxybenzene moiety of **2** extend into a solvent-exposed region without forming additional favorable contacts with BCL-X_L. The absence of such stabilizing interactions may partially explain their lower biochemical potencies relative to Cpd14.

To exclude the possibility that the newly identified inhibitors bind to an alternative site on BCL-X_L, additional docking simulations were performed using docking grids encompassing the entire protein structure. No energetically favorable peripheral binding pocket capable of accommodating either compound was identified, and all predicted binding poses outside the BH3-binding groove were associated with unfavorable binding free energies. These findings provide further support for the proposed binding mechanism in which **1** and **2**

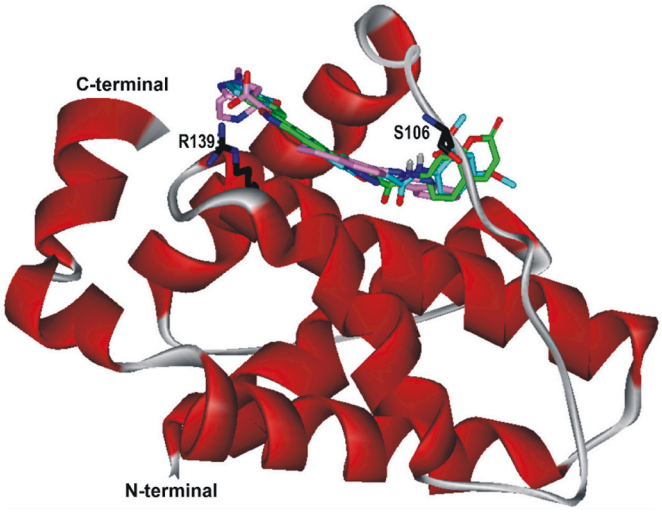


Fig. 6. Predicted binding poses of **1** and **2** in the BH3-binding groove of BCL-X_L, superimposed with the crystallographic binding pose of Cpd14 from the original X-ray structure. Carbon atoms of BCL-X_L, Cpd14, **1**, and **2** are shown in black, pink, green, and cyan, respectively. The key binding-site residues Ser106 and Arg139 are also presented.

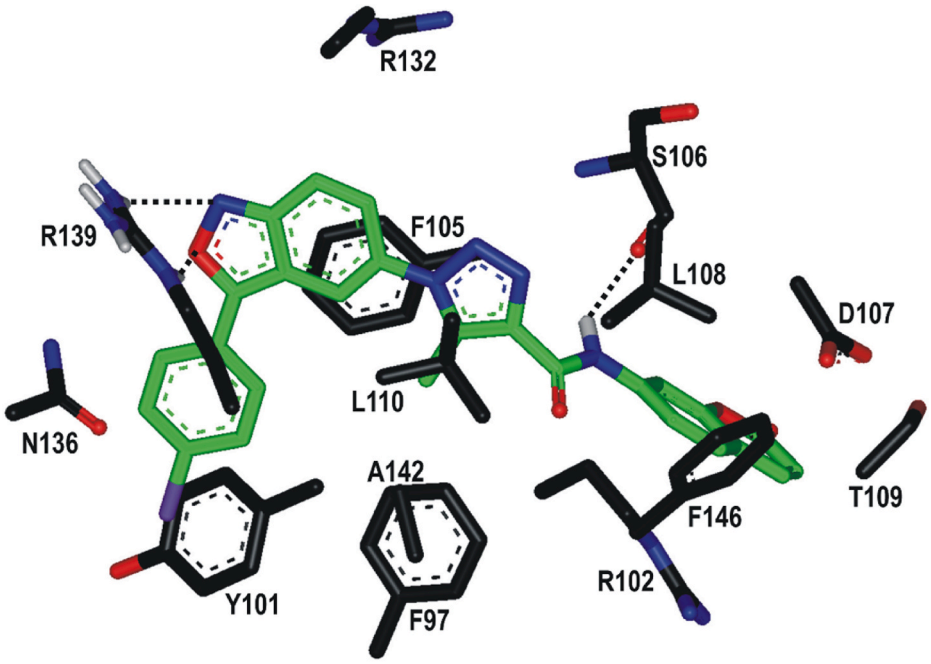


Fig. 7. Predicted binding mode of **1** within the BH3-binding groove of BCL-X_L. The carbon atoms of BCL-X_L and **1** are shown in black and green, respectively. Hydrogen bonds are depicted as dashed lines.

competitively inhibit BH3 peptide binding by occupying the canonical BH3-binding groove of BCL-X_L.

We next examined the intermolecular interactions predicted to stabilize **1** within the BH3-binding groove of BCL-X_L. As shown in Fig. 7, the amide NH group of **1** forms a hydrogen bond with the backbone carbonyl oxygen of Ser106 in its lowest-energy docking pose. This conserved interaction likely serves as an anchor for positioning the ligand within the binding groove, consistent with X-ray crystallographic [17,18,44] and computational studies [45,46] demonstrating the importance of the Ser106 backbone hydrogen bond in BCL-X_L inhibitor binding. In addition, the benzo[c]isoxazole moiety of **1** forms two hydrogen bonds with the guanidinium group of Arg139, resulting in a three-hydrogen-bond network that may contribute substantially to ligand stabilization. The complex is further stabilized by hydrophobic and van der Waals contacts with Phe97, Tyr101, Phe105, Leu108, Thr109, Leu110, Ala142, and Phe146. Collectively, these interactions provide a plausible structural basis for the submicromolar potency of **1**. The predicted binding mode also suggests opportunities for further optimization: structural modifications that extend into adjacent unoccupied regions of the BH3-binding groove while preserving the key interactions with Ser106 and Arg139 may enhance binding affinity and potentially yield more potent BCL-X_L inhibitors.

Fig. 8 shows the predicted binding mode of **2** within the BH3-binding groove of BCL-X_L. In the calculated complex, the amide NH group adjacent to the terminal dimethoxybenzene moiety forms a hydrogen bond with the backbone carbonyl oxygen of Ser106, a key recognition

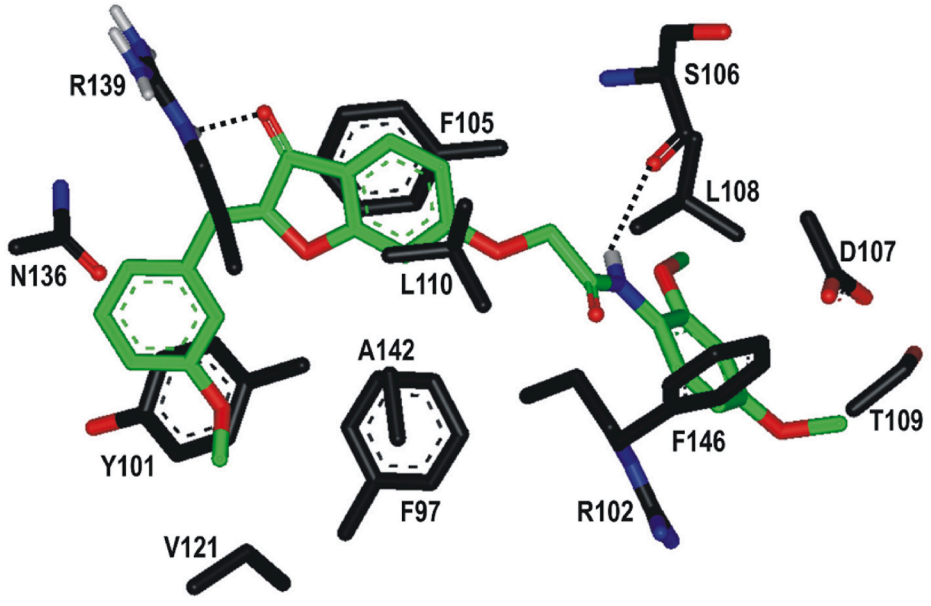


Fig. 8. Calculated docking pose of **2** in the BH3-binding groove of BCL-X_L. Carbon atoms of the protein and ligand are colored black and green, respectively. Hydrogen-bonding interactions are indicated by dotted lines.

element for BCL-X_L inhibitor binding [44–46]. As observed for **1** (Fig. 7), an additional hydrogen bond is formed between the guanidinium group of Arg139 and the carbonyl oxygen of the five-membered ring of **2**, further stabilizing the complex. These directional hydrogen bonds are complemented by extensive hydrophobic contacts with Phe97, Tyr101, Phe105, Leu108, Thr109, Leu110, Val121, Ala142, and Phe146. Overall, the predicted binding mode of **2** closely resembles that of **1**, with both compounds sharing the key hydrogen-bonding interactions with Ser106 and Arg139 and extensive hydrophobic contacts within the BH3-binding groove.

Comparison of the predicted binding modes of **1** and **2** provides a plausible structural explanation for their different biochemical potencies. Although both compounds maintain key hydrogen bonds with Ser106 and Arg139, **1** forms an additional hydrogen bond with Arg139 through its benzo[*c*]isoxazole moiety, resulting in three hydrogen bonds compared with two for **2**. The absence of this additional interaction may contribute to the lower potency of **2**, consistent with its low-micromolar rather than submicromolar activity. Nevertheless, the lower MW of **2** provides greater scope for structural modification, making it an attractive scaffold for further medicinal chemistry optimization while maintaining favorable drug-like properties.

Regarding the predicted binding modes of **1** and **2**, the hydrophobic contacts with Phe105, Leu108, Leu110, and Phe146 are located adjacent to the key hydrogen-bonding network in both complexes (Figs. 7 and 8). These nonpolar residues may reinforce the hydrogen bonds by shielding them from solvent exposure and reducing competition with water molecules, a well-established mechanism for stabilizing protein–ligand interactions [47,48]. This observation suggests that hydrophobic substituents positioned near the key hydrogen-bonding motifs may contribute to the binding affinities of **1** and **2**. Notably, however, neither compound forms a predicted interaction with Tyr195, a residue known to establish van der Waals contacts with many potent BCL-X_L inhibitors [49]. The absence of this interaction may partially account for their lower potencies relative to nanomolar BCL-X_L inhibitors. Accordingly, future structural optimization of **1** and **2** could focus on extending suitable substituents toward Tyr195 to establish additional van der Waals contacts while preserving the key hydrogen-bonding interactions with Ser106 and Arg139.

3.4. Molecular dynamics validation of binding modes

To investigate the dynamic behavior associated with the inhibitory activities of **1** and **2**, MD simulations were performed using the BCL-X_L–**1** and BCL-X_L–**2** complex structures obtained from the docking studies as the initial configurations. The conformational stability of both BCL-X_L and the bound inhibitors in aqueous solution was evaluated by monitoring the time-dependent root-mean-square deviations from the initial production structures ($RMSD_{init}$). The $RMSD_{init}$ values were calculated separately for the C_α atoms of the BCL-X_L backbone and the heavy atoms of each inhibitor to characterize the overall structural fluctuations of the protein and the positional stability of the ligands within the BH3-binding groove, respectively. As shown in Fig. 9, the $RMSD_{init}$ values of the BCL-X_L C_α atoms remained below 2.4 Å throughout the simulations for both complexes and exhibited an overall tendency toward convergence as the simulations progressed. These relatively small deviations indicate that the overall fold of BCL-X_L was well preserved during the MD trajectories, with no substantial conformational rearrangements occurring under the simulation conditions described in the preceding section. The average protein $RMSD_{init}$ values were also similar between the two systems, amounting to 1.752 and 1.812 Å for the BCL-X_L–**1** and BCL-X_L–**2** complexes, respectively. Thus, binding of either inhibitor appears to be compatible with a structurally stable BCL-X_L conformation over the simulation timescale.

The bound ligands exhibited even smaller structural deviations than the protein. Throughout the simulations, the heavy-atom $RMSD_{init}$ values of **1** and **2** fluctuated around approximately 0.5 Å and remained consistently lower than the corresponding C_α $RMSD_{init}$ values of BCL-X_L. Their average $RMSD_{init}$ values were only 0.383 and 0.405 Å, respectively. Such small deviations from the initial docked conformations suggest that both inhibitors remained stably accommodated within the BH3-binding groove and underwent only limited positional and conformational fluctuations during the simulations. These observations therefore provide dynamic support for the binding modes predicted by the docking calculations and indicate that neither compound underwent substantial displacement from its initial binding orientation.

To assess the dynamic stability of the key intermolecular interactions between BCL-X_L and the two identified inhibitors (**1** and **2**), we also monitored the time-dependent variations in the donor–acceptor distances associated with the hydrogen bonds predicted from the docking simulations (Figs. 7 and 8). Specifically, three hydrogen bonds were analyzed for the BCL-X_L–**1** complex and two for the BCL-X_L–**2** complex, involving the backbone amide moiety of Ser106 and the side-chain guanidinium group of Arg139. As shown in Fig. 10a, all three hydrogen bonds in the BCL-X_L–**1** complex appear to remain well preserved throughout most of the 20.4 ns MD simulation. In particular, the N–H···O hydrogen bond formed between the amide moiety of **1** and the backbone carbonyl oxygen of Ser106 is maintained at a donor–acceptor distance of less than 2.5 Å for 94.8% of the simulation time, indicating a highly persistent interaction. Similarly, the N–H···O and N–H···N hydrogen bonds formed between the side-chain guanidinium group of Arg139 and the benzo[c]isoxazole moiety of **1** remain within the 2.5 Å distance criterion [50] for 98.3% and 99.9% of the simulation time,

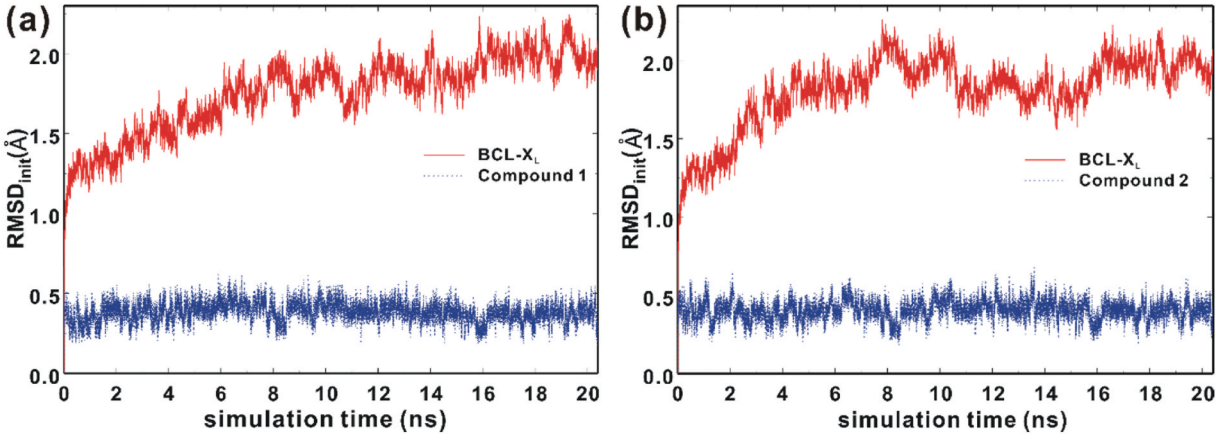


Fig. 9. Time evolution of the $RMSD_{init}$ values calculated for the backbone C_α atoms of BCL-X_L and for the ligand heavy atoms (excluding hydrogens) in the (a) BCL-X_L–**1** and (b) BCL-X_L–**2** complexes, measured relative to their respective initial structures at the start of the production MD simulations.

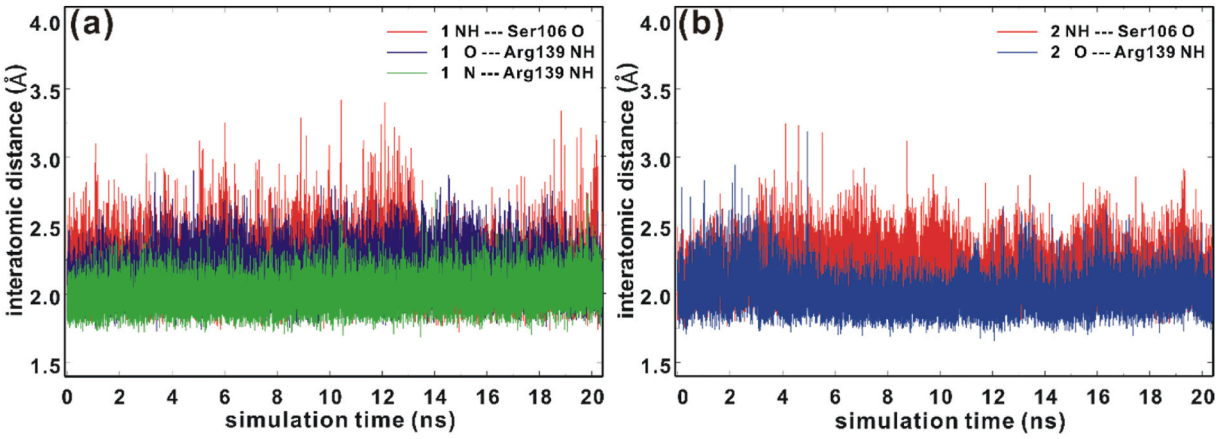


Fig. 10. Time evolution of the interatomic distances corresponding to the hydrogen bonds formed between ligand atoms and Ser106 and Arg139 of BCL-X_L in the (a) BCL-X_L–**1** and (b) BCL-X_L–**2** complexes.

respectively. These results demonstrate that the hydrogen-bonding network predicted for **1** by molecular docking is largely retained under dynamic conditions rather than representing transient interactions associated with a single energy-minimized docking pose.

A comparable degree of hydrogen-bond persistence is observed for the BCL-X_L–**2** complex (Fig. 10b). The N–H···O hydrogen bond between the amide moiety of **2** and the backbone carbonyl oxygen of Ser106 remains within the 2.5 Å distance criterion for 96.6% of the simulation time. Likewise, the hydrogen bond involving the carbonyl oxygen of **2** and the side-chain guanidinium group of Arg139 is maintained for 99.6% of the trajectory. The consistently short donor–acceptor distances and high occupancies of these interactions indicate that **2**, similar to **1**, retains the principal hydrogen-bonding interactions predicted from its docked binding mode during the MD simulation. Taken together, the MD simulation results support the dynamic stability of the docking-derived binding modes of **1** and **2**, with the key hydrogen bonds involving Ser106 and Arg139 persisting for the great majority of the simulation trajectories. The sustained nature of these interactions suggests that they contribute to stabilization of the inhibitors within the BH3-binding groove of BCL-X_L and may therefore represent important molecular determinants underlying their experimentally observed inhibitory activities against BCL-X_L.

However, the relatively short simulation duration of approximately 20 ns may not be sufficient to adequately sample the conformational space accessible to the BCL-X_L–inhibitor complexes. In particular, protein conformational rearrangements and alternative ligand-binding configurations occurring on longer timescales may not have been fully captured. Accordingly, the present MD simulations should be interpreted primarily as an evaluation of the short-term structural stability of the docking-predicted binding modes rather than a comprehensive characterization of the conformational dynamics and thermodynamic equilibrium of the complexes.

3.5. Structure-based optimization strategy for the newly identified BCL-X_L inhibitors

The successful identification of **1** and **2** demonstrates that combining the AutoDock scoring function with a structural filter requiring key hydrogen bonds with Ser106 and Arg139 provides an effective strategy for discovering inhibitors of peptide binding to BCL-X_L. This structure-based approach may also facilitate the optimization of **1** and **2** into more potent inhibitors through iterative *de novo* design. Derivatives would be generated based on their predicted BCL-X_L binding modes, with emphasis on preserving the critical hydrogen bonds while introducing substituents capable of forming additional favorable interactions within the BH3-binding groove. The resulting virtual compounds could then be prioritized using AutoDock scores and the Ser106/Arg139/Tyr195 interaction constraints, followed by synthesis and experimental evaluation of the most promising candidates. As a continuation of this work, we plan to pursue a collaborative lead-optimization program integrating computational design, chemical synthesis, biochemical evaluation, and SAR analysis to develop more potent BCL-X_L inhibitors.

4. Conclusions

BCL-X_L is an attractive anticancer target, but the large and shallow nature of its BH3-binding groove poses a substantial challenge to the discovery of potent, drug-like small-molecule inhibitors. In this study, structure-based virtual screening incorporating both docking scores and key interaction constraints identified two structurally novel BCL-X_L inhibitors, **1** and **2**, with IC_{50} values of 0.34 and 2.51 μM, respectively. Both compounds possess relatively low MWs and represent previously unreported scaffolds, providing considerable chemical space for further optimization. The results of docking and MD simulations suggested that both inhibitors occupy the canonical BH3-binding groove and maintain the targeted hydrogen bonds with Ser106 and Arg139, together with extensive hydrophobic interactions. The greater potency of **1** may be partly attributed to an additional hydrogen bond with Arg139 through its benzo[c]isoxazole moiety. Importantly, neither compound was predicted to interact with Tyr195, suggesting that extending appropriate substituents toward this residue while preserving the key Ser106 and Arg139 interactions may provide a rational strategy for improving potency. Overall, these findings demonstrate the utility of incorporating key interaction constraints into docking-based virtual screening for challenging protein–protein interaction targets and establish **1** and **2** as promising starting scaffolds for further BCL-X_L inhibitor development. Future studies will focus on structure-guided optimization and systematic SAR exploration to achieve nanomolar potency, followed by evaluation of cellular activity, pharmacokinetic properties, and BCL-X_L-associated toxicity to determine their potential for further preclinical development.

CRediT authorship contribution statement

Hyunjin Kim: Writing – original draft, Visualization, Validation, Software, Investigation, Data curation. **Ahyoung Jang:** Visualization, Software, Investigation, Data curation. **Sungwoo Hong:** Validation, Supervision. **Seong Eon Ryu:** Writing – review & editing, Validation, Supervision, Methodology, Conceptualization. **Hwangseo Park:** Writing – review & editing, Validation, Supervision, Methodology, Investigation, Conceptualization.

Declaration of generative AI and AI-assisted technologies

The authors used an AI-assisted tool (ChatGPT) solely to correct typographical and grammatical errors throughout the manuscript. The authors take full responsibility for the accuracy, integrity, and content of the work.

Declaration of competing interest

The authors declare that they have no known competing financial interests or personal relationships that could have appeared to influence the work reported in this paper.

Acknowledgements

This work was supported by Basic Science Research Program (RS-2025-00563429) through the National Research Foundation of Korea and by the Bio & Medical Technology Development Program (RS-2021-NR056525).

Data availability

All computational and experimental data will be available upon request.

References

[1] M. Vogler, Y. Braun, V.M. Smith, M.-A. Westhoff, R.S. Pereira, N.M. Pieper, M. Anders, M. Callens, T. Vervliet, M. Abbas, S. Macip, R. Schmid, G. Bultynck, M. J.S. Dyer, The BCL2 family: from apoptosis mechanisms to new advances in targeted therapy, Signal Transduct. Targeted Ther. 10 (2025) 91.

[2] M. Li, D. Wang, J. He, L. Chen, H. Li, Bcl-XL: a multifunctional anti-apoptotic protein, Pharmacol. Res. 151 (2020) 104547.

[3] S. Choi, Z. Chen, L.H. Tang, Y. Fang, S.J. Shin, N.C. Panarelli, Y.-T. Chen, Y. Li, X. Jiang, Y.-C.N. Du, Bcl-xL promotes metastasis independent of its anti-apoptotic activity, Nat. Commun. 7 (2016) 10384.

[4] E.J. Hennessy, Selective inhibitors of Bcl-2 and Bcl-xL: balancing antitumor activity with on-target toxicity, Bioorg. Med. Chem. Lett. 26 (2016) 2105–2114.

[5] A. Ashkenazi, W.J. Fairbrother, J.D. Leverson, A.J. Souers, From basic apoptosis discoveries to advanced selective BCL-2 family inhibitors, Nat. Rev. Drug Discov. 16 (2017) 273–284.

[6] J.D. Leverson, D.C. Phillips, M.J. Mitten, E.R. Boghaert, D. Diaz, S.K. Tahir, L. D. Belmont, P. Nimmer, Y. Xiao, X.M. Ma, K.N. Lowes, P. Kovar, J. Chen, S. Jin, M. Smith, J. Xue, H. Zhang, A. Oleksijew, T.J. Magoc, K.S. Vaidya, D.H. Albert, J. M. Tarrant, N. La, L. Wang, Z.-F. Tao, M.D. Wendt, D. Sampath, S.H. Rosenberg, C. Tse, D.C.S. Huang, W.J. Fairbrother, S.W. Elmore, A.J. Souers, Exploiting selective BCL-2 family inhibitors to dissect cell survival dependencies and define improved strategies for cancer therapy, Sci. Transl. Med. 7 (2015), 279ra40.

[7] G. Lessene, P.E. Czabotar, P.M. Colman, BCL-2 family antagonists for cancer therapy, Nat. Rev. Drug Discov. 7 (2008) 989–1000.

[8] P.E. Czabotar, A.J. Garcia-Saez, Mechanisms of BCL-2 family proteins in mitochondrial apoptosis, Nat. Rev. Mol. Cell Biol. 24 (2023) 732–748.

[9] E.F. Lee, W.D. Fairlie, The structural biology of Bcl-xL, Int. J. Mol. Sci. 20 (2019) 2234.

[10] A.M. Petros, A. Medek, D.G. Nettesheim, D.H. Kim, H.S. Yoon, K. Swift, E. D. Matayoshi, T. Oltersdorf, S.W. Fesik, Solution structure of the antiapoptotic protein Bcl-2, Proc. Natl. Acad. Sci. USA 98 (2001) 3012–3017.

[11] T. Oltersdorf, S.W. Elmore, A.R. Shoemaker, R.C. Armstrong, D.J. Augeri, B. A. Belli, M. Bruncko, T.L. Deckwerth, J. Dinges, P.J. Hajduk, M.K. Joseph, S. Kitada, S.J. Korsmeyer, A.R. Kunzer, A. Letai, C. Li, M.J. Mitten, D. G. Nettesheim, S. Ng, P.M. Nimmer, J.M. O'Connor, A. Oleksijew, A.M. Petros, J. C. Reed, W. Shen, S.K. Tahir, C.B. Thompson, K.J. Tomaselli, B. Wang, M.D. Wendt, H. Zhang, S.W. Fesik, S.H. Rosenberg, An inhibitor of Bcl-2 family proteins induces regression of solid tumours, Nature 435 (2005) 677–681.

[12] E.F. Lee, P.E. Czabotar, B.J. Smith, K. Deshayes, K. Zobel, P.M. Colman, W. D. Fairlie, Crystal structure of ABT-737 complexed with Bcl-xL: implications for selectivity of antagonists of the Bcl-2 family, Cell Death Differ. 14 (2007) 1711–1713.

[13] S.B. Balachander, S.W. Criscione, K.F. Byth, J. Cidado, A. Adam, P. Lewis, T. Macintyre, S. Wen, D. Lawson, K. Burke, T. Lubinski, J.W. Tyner, S.E. Kurtz, S. K. McWeeney, J. Varnes, R.B. Diebold, T. Gero, S. Ioannidis, E.J. Hennessy, W. McCoull, J.C. Saeh, A. Tabatabai, O. Tavana, N. Su, A. Schuller, M.J. Garnett, P. Jaaks, E.A. Coker, G.P. Gregory, A. Newbold, R.W. Johnstone, E. Gangl, M. Wild, M. Zinda, J.P. Secrist, B.R. Davies, S.E. Fawell, F.D. Gibbons, AZD4320, a dual inhibitor of Bcl-2 and Bcl-xL, induces tumor regression in hematologic cancer models without dose-limiting thrombocytopenia, Clin. Cancer Res. 26 (2020) 6535–6549.

[14] G. Lessene, P.E. Czabotar, B.E. Sleebs, K. Zobel, K.N. Lowes, J.M. Adams, J.B. Baell, P.M. Colman, K. Deshayes, W.J. Fairbrother, J.A. Flygare, P. Gibbons, W.J. A. Kersten, S. Kulasegaram, R.M. Moss, J.P. Parisot, B.J. Smith, I.P. Street, H. Yang, D.C.S. Huang, K.G. Watson, Structure-guided design of a selective BCL-XL inhibitor, Nat. Chem. Biol. 9 (2013) 390–397.

[15] B.E. Sleebs, W.J.A. Kersten, S. Kulasegaram, G. Nikolakopoulos, E. Hatzis, R. M. Moss, J.P. Parisot, H. Yang, P.E. Czabotar, W.D. Fairlie, E.F. Lee, J.M. Adams, L. Chen, M.F. van Delft, K.N. Lowes, A. Wei, D.C.S. Huang, P.M. Colman, I.P. Street, J.B. Baell, K. Watson, G. Lessene, Discovery of potent and selective benzothiazole hydrazone inhibitors of BCL-XL, J. Med. Chem. 56 (2013) 5514–5540.

[16] L. Wang, G.A. Doherty, A.S. Judd, Z.-F. Tao, T.M. Hansen, R.R. Frey, X. Song, M. Bruncko, A.R. Kunzer, X. Wang, M.D. Wendt, J.A. Flygare, N.D. Catron, R. A. Judge, C.H. Park, S. Shekhar, D.C. Phillips, P. Nimmer, M.L. Smith, S.K. Tahir, Y. Xiao, J. Xue, H. Zhang, P.N. Le, M.J. Mitten, E.R. Boghaert, W. Gao, P. Kovar, E. F. Choo, D. Diaz, W.J. Fairbrother, S.W. Elmore, D. Sampath, J.D. Leverson, A. J. Souers, Discovery of A-1331852, a first-in-class, potent, and orally-bioavailable BCL-XL inhibitor, ACS Med. Chem. Lett. 11 (2020) 1829–1836.

[17] Z.-F. Tao, L. Hasvold, L. Wang, X. Wang, A.M. Petros, C.H. Park, E.R. Boghaert, N. D. Catron, J. Chen, P.M. Colman, P.E. Czabotar, K. Deshayes, W.J. Fairbrother, J. A. Flygare, S.G. Hymowitz, S. Jin, R.A. Judge, M.F.T. Koehler, P.J. Kovar, G. Lessene, M.J. Mitten, C.O. Ndubaku, P. Nimmer, H.E. Purkey, A. Oleksijew, D. C. Phillips, B.E. Sleebs, B.J. Smith, M.L. Smith, S.K. Tahir, K.G. Watson, Y. Xiao, J. Xue, H. Zhang, K. Zobel, S.H. Rosenberg, C. Tse, J.D. Leverson, S.W. Elmore, A. J. Souers, Discovery of a potent and selective BCL-XL inhibitor with in vivo activity, ACS Med. Chem. Lett. 5 (2014) 1088–1093.

[18] M.P. Timari, A. Paczal, A. Herner, M. Molnar, Z. Madarasz, M. Nyerges, S. T. Bedford, T. Brooks, J. Davidson, Z. Daniels, M. Dodsworth, P. Dokurno, J. B. Murray, R. Parsons, E. Sanders, J. Smith, P. Webb, N. Whitehead, R.E. Hubbard, J.-B. Starck, A.L. Maragno, G. Le Toumelin-Braizat, L. Bresson, F. Rocchetti, D. Demarles, F. Colland, O. Geneste, A. Kotschy, T. Novak, Structure-based discovery of potent BCL-XL inhibitors through rescaffolding, J. Med. Chem. 69 (2026) 14804–14818.

[19] A. Aguilar, H. Zhou, J. Chen, L. Liu, L. Bai, D. McEachern, C.-Y. Yang, J. Meagher, J. Stuckey, S. Wang, A potent and highly efficacious Bcl-2/Bcl-xL inhibitor, J. Med. Chem. 56 (2013) 3048–3067.

[20] J. Chen, H. Zhou, A. Aguilar, L. Liu, L. Bai, D. McEachern, C.-Y. Yang, J.L. Meagher, J.A. Stuckey, S. Wang, Structure-based discovery of BM-957 as a potent small-molecule inhibitor of Bcl-2 and Bcl-xL capable of achieving complete tumor regression, J. Med. Chem. 55 (2012) 8502–8514.

[21] Z.-F. Tao, X. Wang, J. Chen, J.P. Ingram, S. Jin, R.A. Judge, P.J. Kovar, C. Park, C. Sun, B.D. Wakefield, L. Zhou, H. Zhang, S.W. Elmore, D.C. Phillips, A.S. Judd, J. D. Leverson, A.J. Souers, Structure-based design of A-1293102, a potent and selective BCL-XL inhibitor, ACS Med. Chem. Lett. 12 (2021) 1011–1016.

[22] R. Fonseca, Y.X. Zhu, P.L. Bergsagel, M. Chesi, A. Pandey, K. Mangalaparthi, Y. Chen, F. Tan, S.P. Anthony, Y. Chen, Y. Shen, B. Dai, E. Braggio, R. Fonseca, LP-118, a novel BCL2 inhibitor, shows potent in vitro anti-myeloma activity, Blood 140 (2022) 7129–7130.

[23] W.D. Fairlie, E.F. Lee, Targeting the BCL-2-regulated apoptotic pathway for the treatment of solid cancers, Biochem. Soc. Trans. 49 (2021) 2397–2410.

[24] S. Khan, X. Zhang, D. Lv, Q. Zhang, Y. He, P. Zhang, X. Liu, D. Thummuri, Y. Yuan, J.S. Wiegand, J. Pei, W. Zhang, A. Sharma, C.R. McCurdy, V.M. Kuruvilla, N. Baran, A.A. Ferrando, Y.-m. Kim, A. Rogojina, P.J. Houghton, G. Huang, R. Hromas, M. Konopleva, G. Zheng, D. Zhou, A selective BCL-XL PROTAC degrader achieves safe and potent antitumor activity, Nat. Med. 25 (2019) 1938–1947.

[25] P. Zhang, X. Zhang, X. Liu, S. Khan, D. Zhou, G. Zheng, PROTACs are effective in addressing the platelet toxicity associated with BCL-XL inhibitors, Explor. Target, Antitumor Ther 1 (2020) 259–272.

[26] E.F. Lee, W.D. Fairlie, Discovery, development and application of drugs targeting BCL-2 pro-survival proteins in cancer, Biochem. Soc. Trans. 49 (2021) 2381–2395.

[27] D. Park, A.T. Magis, R. Li, T.K. Owonikoko, G.L. Sica, S.-Y. Sun, S.S. Ramalingam, F.R. Khuri, W.J. Curran, X. Deng, Novel small-molecule inhibitors of Bcl-XL to treat lung cancer, Cancer Res. 73 (2013) 5485–5496.

[28] S.Y. Huang, S.Z. Grinter, X. Zou, Scoring functions and their evaluation methods for protein-ligand docking: recent advances and future directions, Phys. Chem. Chem. Phys. 12 (2010) 12899–12908.

[29] C.A. Lipinski, F. Lombardo, B.W. Dominy, P.J. Feeney, Experimental and computational approaches to estimate solubility and permeability in drug discovery and development settings, Adv. Drug Deliv. Rev. 23 (1997) 3–25.

[30] C.A. Lipinski, Lead- and drug-like compounds: the rule-of-five revolution, Drug Discov. Today Technol. 1 (2004) 337–341.

[31] J. Gasteiger, C. Rudolph, J. Sadowski, Automatic generation of 3D-atomic coordinates for organic molecules, Tetrahedron Comput. Methodol. 3 (1990) 537–547.

[32] J. Gasteiger, M. Marsili, Iterative partial equalization of orbital electronegativity–a rapid access to atomic charges, Tetrahedron 36 (1980) 3219–3228.

[33] G.M. Morris, D.S. Goodsell, R.S. Halliday, R. Huey, W.E. Hart, R.K. Belew, A. J. Olson, Automated docking using a Lamarckian genetic algorithm and an empirical binding free energy function, J. Comput. Chem. 19 (1998) 1639–1662.

[34] J.W. Ponder, D.A. Case, Force fields for protein simulations, Adv. Protein Chem. 66 (2003) 27–85.

[35] E.L. Mehler, T. Solmajer, Electrostatic effects in proteins: comparison of dielectric and charge models, Protein Eng. 4 (1991) 903–910.

[36] H. Kang, H. Choi, H. Park, Prediction of molecular solvation free energy based on the optimization of atomic solvation parameters with genetic algorithm, J. Chem. Inf. Model. 47 (2007) 509–514.

[37] T. Fox, P.A. Kollman, Application of the RESP methodology in the parametrization of organic solvents, J. Phys. Chem. B 102 (1998) 8070–8079.
[38] H. Zhang, P. Nimmer, S.H. Rosenberg, S.-C. Ng, M. Joseph, Development of a high-throughput fluorescence polarization assay for Bcl-xL, Anal. Biochem. 307 (2002) 70–75.
[39] M. Kontoyianni, L.M. McClellan, G.S. Sokol, Evaluation of docking performance: comparative data on docking algorithms, J. Med. Chem. 47 (2004) 558–565.
[40] J.B. Baell, G.A. Holloway, New substructure filters for removal of pan assay interference compounds (PAINS) from screening libraries and for their exclusion in bioassays, J. Med. Chem. 53 (2010) 2719–2740.
[41] J.B. Baell, J.W.M. Nissink, Seven year itch: pan-assay interference compounds (PAINS) in 2017—utility and limitations, ACS Chem. Biol. 13 (2018) 36–44.
[42] P. Banerjee, E. Kemmler, M. Dunkel, R. Preissner, ProTox 3.0: a webserver for the prediction of toxicity of chemicals, Nucleic Acids Res. 52 (2024) W513–W520.
[43] P. Banerjee, A.O. Eckert, A.K. Schrey, R. Preissner, ProTox-II: a webserver for the prediction of toxicity of chemicals, Nucleic Acids Res. 46 (2018) W257–W263.
[44] M.F.T. Koehler, P. Bergeron, E.F. Choo, K. Lau, C. Ndubaku, D. Dudley, P. Gibbons, B.E. Sleebs, C.S. Rye, G. Nikolakopoulos, C. Bui, S. Kulasegaram, W.J.A. Kersten, B. J. Smith, P.E. Czabotar, P.M. Colman, D.C.S. Huang, J.B. Baell, K.G. Watson, L. Hasvold, Z.-F. Tao, L. Wang, A.J. Souers, S.W. Elmore, J.A. Flygare, W. J. Fairbrother, G. Lessene, Structure-guided rescaffolding of selective antagonists of BCL-XL, ACS Med. Chem. Lett. 5 (2014) 662–667.
[45] J. Luan, B. Hu, S. Wang, H. Liu, S. Lu, W. Li, X. Sun, J. Shi, J. Wang, Selectivity mechanism of BCL-XL/2 inhibition through in silico investigation, Phys. Chem. Chem. Phys. 24 (2022) 17105–17115.
[46] N. Wakui, R. Yoshino, N. Yasuo, M. Ohue, M. Sekijima, Exploring the selectivity of inhibitor complexes with Bcl-2 and Bcl-XL: a molecular dynamics simulation approach, J. Mol. Graph. Model. 79 (2018) 166–174.
[47] P. Schmidtke, F.J. Luque, J.B. Murray, X. Barril, Shielded hydrogen bonds as structural determinants of binding kinetics: application in drug design, J. Am. Chem. Soc. 133 (2011) 18903–18910.
[48] L. Muley, B. Baum, M. Smolinski, M. Freindorf, A. Heine, G. Klebe, D.G. Hangauer, Enhancement of hydrophobic interactions and hydrogen bond strength by cooperativity: synthesis, modeling, and molecular dynamics simulations of a congeneric series of thrombin inhibitors, J. Med. Chem. 53 (2010) 2126–2135.
[49] P. Priya, A. Maity, S. Majumdar, S.G. Dastidar, Interactions between Bcl-xL and its inhibitors: insights into ligand design from molecular dynamics simulation, J. Mol. Graph. Model. 59 (2015) 1–13.
[50] I.K. McDonald, J.M. Thornton, Satisfying hydrogen bonding potential in proteins, J. Mol. Biol. 238 (1994) 777–793.